Proceedings of ICFDP9:
Ninth International Congress of Fluid Dynamics & Propulsion
December 18-21, 2008, Alexandria, Egypt

ICFDP9-EG-243

THEORETICAL AND EXPERIMENTAL STUDY OF CENTRIFUGAL COMPRESSOR IMPELLERS

A. Elnashar, Dr., Egyptian armed forces, E-mail: amrnashar2@yahoo.com, Tel.: 02/0127773040.

Khaled. M. S. Eldalil, Dr. Lecturer, Mech. Eng. Dept, Tanta Univ., Egypt, and R&D Consultant, E-mail: eldalil01@msn.com, Tel.: 02/012587770

A. Hashim, As. Prof Cairo University, Faculty of Eng, Egypt, Aeronautical Eng. Dept, E-mail: aafhashem@yahoo.com, Tel:02/0107976289

M. M. Abdelrahman, Prof, Cairo Univ., Faculty of Eng, Director of Aeronautical Eng. Dept., Egypt, Tel: 02/0123196569
E-mail: dr_madbouli@hotmail.com,

1. ABSTRACT

A test rig has been built for determining a centrifugal compressor impeller flow field characteristic parameters. The compressor is working with a gas turbine engine of type 4M-1 (APU), which has a maximum speed of rotation of 27600 rpm. The engine shaft was being driven by a variable speed electric motor as a cold running test of the engine. The total and static pressures, and temperatures were measured at the impeller inlet, outlet, and in the collector, as well as the speed of rotation and mass flow rates. Whereas, the impeller efficiency, slip factor and aerodynamic blockage were calculated at every measured point. The mass flow rate is varied by using a throttling gate, from its maximum to nearly surge point at each speed, where the surge symptoms start to appear. The mass flow rates and the speeds of rotation are corrected according to the standard ambient pressure and temperature. A loss model was developed using the basic fluid equations aided by some empirical relations, then it was applied on the measured case. An aerodynamic 3-D viscous flow analysis was made using "CFX-BladeGen" software package. A comparison between measured and theoretically calculated results showed a good agreement.

KEYWORDS:

Centrifugal compressor impeller, Experimental, Measurements, Loss model, Efficiency, Performance prediction.

2. INTRODUCTION

The centrifugal compressor is one of the most important types of turbo-machinery applications. Its industrial applications are wide, including many critical fields such as pharmacological, chemical, and nutrition fields. It is commonly used in small gas turbine engines, where using axial compressors is not very efficient due to the relatively big tip clearance at its last stages. Generally, the centrifugal compressor has many advantages, it has high pressure ratio per stage with reasonable efficiency, and having high resistance to foreign object damage. In addition, its production is easy and it has less number of parts than the axial compressor.

The nature of the flow inside the centrifugal compressor is a three-dimensional, turbulent, and viscous flow; it represents a challenge to the designer of such part. In addition, existence of many secondary flows represents another difficulty to be added to the design process.

The design usually starts by using the basic fluid equations to layout the main dimensions, and then the process continued using 2-D and 3-D CFD solvers to determine the flow parameters and dimensions more accurately.

Experimental measurements of the flow parameters of new designed compressors are necessary to evaluate the actual performance. It is an indispensable step, even if powerful and accurate tools were used in the design process. In addition, measurements may be performed for assessment of loss models and fluid flow solvers. Eckardet [1] used a laser velocimeter to measure the flow velocity and determine the performance

parameters of a centrifugal compressor. Mizuki et al. [2] used yaw probes distributed along the channel between centrifugal compressor blades, to measure the total and static pressures. That author used two groups of probes, an attached probes on the hub and blade walls (rotating with the impeller), and fixed probes (on the shroud).

The loss models are very efficient tools, which can help in designing and evaluating compressors. They are simulating losses facing the real flow by using the basic fluid equations aided by some empirical relations. A trustable loss model can help saving money and time of experimental work needed for evaluation, especially when the operating conditions are similar to those that the loss model was adopted for.

In the present work, detailed measurements of Elnashar [3] are explained, where total pressures, static pressures, and total temperature at the impeller exit, besides the inlet total conditions are measured. In addition, a loss model is proposed, which uses basic fluid flow equations together with some empirical formulas, to determine the performance parameters of the impeller. Finally, a three dimensional viscous fluid flow solution is presented, which uses a commercial Navier-stokes solver. The aim of the present work is to construct a wide band spectrum comparison of the experimentally obtained impeller characteristic parameters and those, which are obtained theoretically by the proposed loss model and 3-D viscous fluid flow solver. In addition, the slip factor and aerodynamic blockage were investigated.

3- EXPERIMENTAL WORK

3.1. Experimental Setup

The experimental setup layout is shown in figure (1) using a photocopy from two sides complimented by a sketch drawing, it consists of the following components:

A gas turbine engine of type (4-M1) has a single stage centrifugal compressor and single stage radial turbine. The engine function is to derive an auxiliary power unit to provide electric power for field mobile applications. The electric generator has a front gearbox (30) of type (SAB), which is equipped with two inputs to transmit power to the generator by two alternative ways. First, by using turbo-shaft engine (4-M1) internal gearbox with 6000 rpm (29A) or by using the tractor diesel engine gearbox with 1500 rpm (29B).

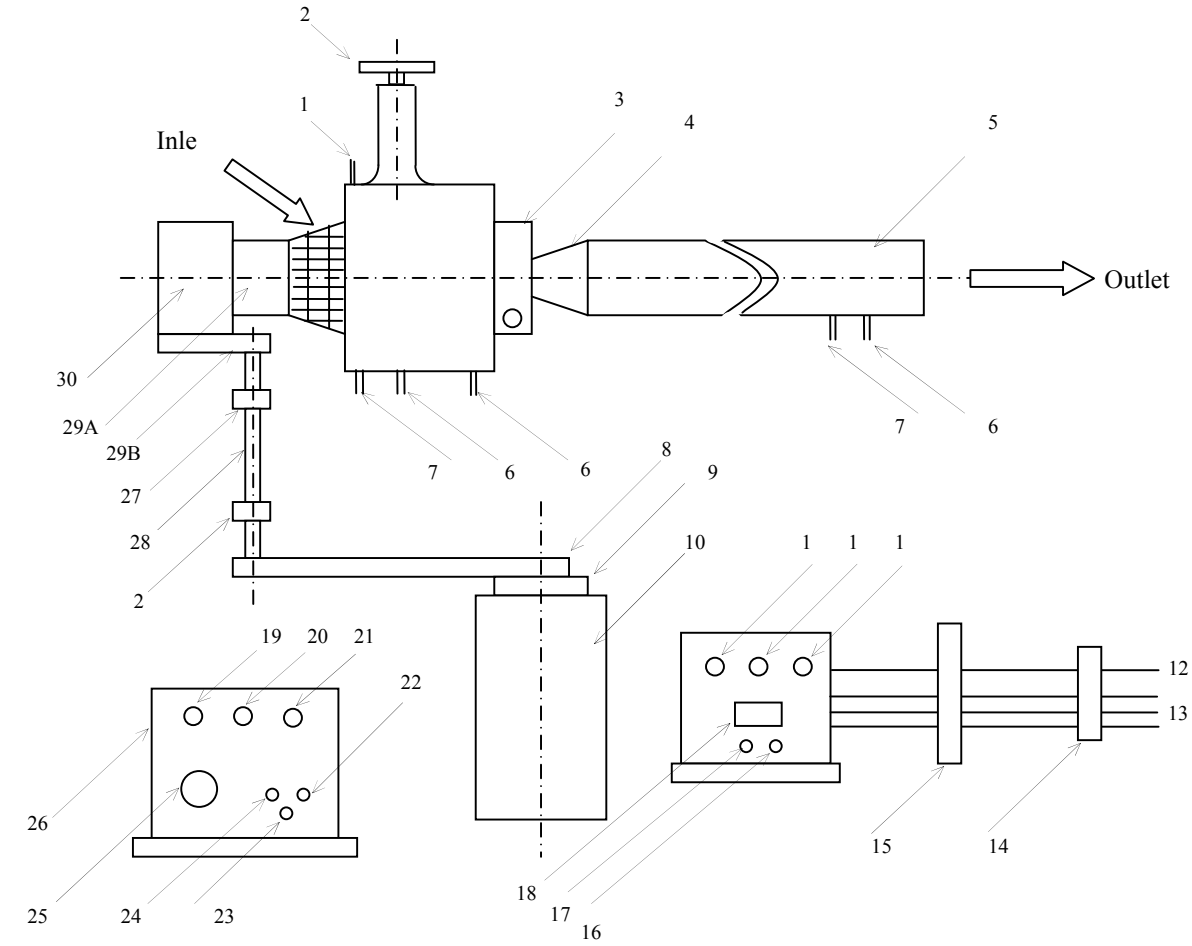

1- Total temperature sensor
2- Choking gate
3- Engine exhaust tube
4- Adaptor
5- Exhaust pipe
6- Total pressure sensor
7- Static pressure sensor
8- Sprocket 4:1 ratio
9- Electric motor gear box
10- Electric motor
11- Volt meter
12- Neutral line
13- The three high voltage lines
14- Circuit breaker
15- Transformer 500-380 volt
16- Increase speed button
17- Reduce speed button
18- Circuit breaker
19- Engine RPM
20- Engine oil temperature
21- Engine oil pressure
22- Engine run
23- Engine stop
24- Engine cold running
25- Total pressure gauge
26- Engine instrument panel
27- Bearing
28- Transmission shaft
29A- Coupling from gasturbine engine.
29B- Coupling from Diesel engine
30- Coupling to electric generator
31- Cooling blower

Fig (1) Experimental setup layout

There is a special coupling at each power input connection, which ensures that driving of the electric generator by one engine will not rotate the other engine (one directional coupling). The test rig is organized such that the diesel engine and the electric generator are discarded, where the one-directional coupling of the turbo-shaft engine was changed to become able to transmit load in both directions.

A Schrage motor (10) of power 125 KW is utilized to derive the system, where its output was connected to external sprocket transmission (8) of speed ratio of (4:1) to raise the maxmaximum driving speed of rotation from 712 to 2848 at the inlet side (29B) of the gearbox (30). The gearbox (30) and the engine internal gearbox are responsible for increasing the gas turbine shaft speed to 27600 rpm. A forced air stream is blown to cool down and keep the gearbox (30) temperature almost constant. In addition, an electric control panel is used to control the speed of the Schrage motor. An electronic beam hand-held stroboscope is used to measure the speed of rotation of the Schrage motor shaft, besides a belt-in electric tachometer (20) to measure the engine speed of rotation. The engine instrumentation panel (22) collects the parameters readings of the gas turbine engine.

A pressure and temperature sensors are mounted at the impeller outlet, collector, and outlet exhaust tube to measure the total pressures, static pressures, and total temperatures. At station (2), the total pressure was measured by using one hole Pitot tube of diameter about (1.2 mm) and at every measuring point, the sensor is turned around its axis until reaching the maximum steady state reading. The Pitot tube is moved laterally in the vainless diffuser width from wall to wall through five points equally spaced, and then the average value is calculated by a numerical integration. The static pressure is measured through a hole in the vaneless diffuser casing at radial distance located 6mm downstream of the total pressure measuring point. The total temperature was measured using a special probe that nearly stagnate the flow, where a k-type thermocouple junction is fixed inside, the dimensions of the probe is made according to specifications stated by Eldalil et al. [4].

The total temperature and total pressure at station (2) is affected severely by the impeller exit jet-wake pattern especially at higher speeds of rotation. Therefore, the total temperatures and total pressures are measured in the collector (station 3), then the total temperatures and pressures T_{o2}, P_{o2} are evaluated by accounting for the diffuser losses.

The mass flow rates are measured in the exhaust duct (station 4), which is equipped with flow straightener in its entrance. The measuring probes are placed at a location after the straightener by a distance long enough to ensure that the flow will become fully developed. The dynamic and static pressures are measured by a calibrated pitot-tube. The total temperature is measured using a probe similar to that used at the impeller exit. The engine mass flow rate is calculated using the previous measured values through the substitution in the continuity equation**.**

$$W_2 = \sqrt{2\,Cp\ (T_{o2r} - T_{s2})} \qquad (9)$$

3.2. Impeller Characteristic Parameters Calculations

The main objective of this part is to determine the impeller performance characteristics parameters in order to construct the impeller map. The mass flow rates and speeds of rotation are corrected by using equations (1) and (2). The total pressure, was measured just at the compressor outlet (station 2), where the point of measurement of static pressure was far from the impeller exit (6mm) downstream in the vaneless diffuser. At this distance, static pressure is considerably affected, due to the change of radius and channel width, consequently the cross-sectional area.

The continuity equation (3), in the dimensionless form is used to calculate the Mach number and consequently static pressure (P_{S2}) for a known value of static pressure at station (22), considering constant total pressure, total temperature, blockage, flow angle and mass flow rate. Finally, the total efficiency of the impeller is calculated by using equation (4).

where, $AR_2 = 2\,\pi\,r\,b$, r = 123 mm, b = 16 mm

$$n_{cor} = n * \sqrt{\frac{T_{o1}}{288}} \qquad (1)$$

$$\dot{m}_{cor} = \dot{m}\ \frac{101325}{p_{o1}} \sqrt{\frac{T_{o1}}{288}} \qquad (2)$$

$$\frac{\dot{m}\sqrt{RTo/\gamma}}{AR_2 \cos\alpha\ Bl\ Po} = M\left(1+\frac{\gamma-1}{2}M^2\right)^{-3} \qquad (3)$$

$$\eta_{tt} = \frac{\left(\frac{p_{o2}}{p_{o1}}\right)^{\frac{\gamma-1}{\gamma}} - 1}{\left(\frac{T_{o2}}{T_{o1}}\right) - 1} \qquad (4)$$

Further more, the calculations continued to determine the slip factor as described by Wisner [5] and the aerodynamic blockage using equation (5) as defined by Pampreen [6] throw the relations stated by Whitfield et al. [7], and Cumpsty [8].

Determination of (α_2) requires solving the outlet velocity triangle figure (2) using equations (6), (7) and (8), whereas T_{S2} is determined using P_{O2} T_{o2}, and P_{s2}.

Solution of the previous equations (7, and 8) requires determination of (W_2) using equation (9), which in turn

$$\gamma_2 = \cos^{-1}\left(\frac{U_2^2 + C_2^2 - W_2^2}{2U_2C_2}\right) \qquad (7)$$

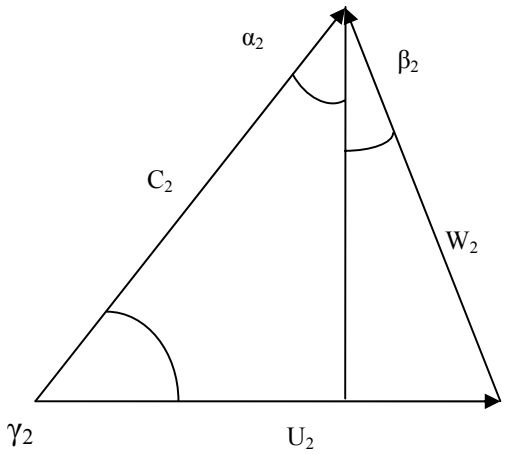

Fig (2) Impeller outlet velocity triangle

$$\alpha_2 = 90 - \gamma_2 \qquad (8)$$

requires the value of exit total relative temperature using the concept of constant rothalpy explained by Matengly [9] using equation (10).Solving equation (10) requires solving inlet velocity triangle at first to determine (W_1), starting by solving equation (11) to determine the inlet Mach number for given inlet area and total conditions. Following, using the continuity equation for known mass flow rate, inlet area, and density (using equations 12 and 13), the inlet velocity could be determined, Consequently the inlet relative total enthalpy can be calculated using inlet peripheral velocity (U_1) at mean radius.

The slip factor could be determined using the following

relations (equations 14, 15, 16, and 17) as follows:

$$Bl = \dot{m} R T_{s2} / \left(p_{s2} AR_2 C_2 \cos(\alpha_2)\right) \qquad (5)$$

$$C_2 = \sqrt{2C_p\left(T_{o2} - T_{s2}\right)} \qquad (6)$$

$$T_{o2r} = \frac{U_2^2 - U_1^2}{2C_p} + T_{o1r} \qquad (10)$$

$$\rho_1 = \frac{\rho_{o1}}{\left(1 + \frac{\gamma - 1}{2} M_1^2\right)^{-2.5}} \qquad (12)$$

$$\frac{\dot{m}\left(RT_{o1}/\gamma\right)^{0.5}}{AR_1 p_{o1}} = M_1\left(1 + \frac{\gamma - 1}{2} M_1^2\right)^{-3} \qquad (11)$$

$$\rho_{o1} = \frac{p_{o1}}{RT_{o1}} \qquad (13)$$

$$\mu = 1 - \frac{\left(C_{\theta 2\,\mathrm{inf}} - C_{\theta 2}\right)}{U_2} \qquad (14)$$

where $\beta_{B2} = -5$ Deg

$C_{2\theta\,\mathrm{inf}} = U_2 + C_{m2} \tan(\beta_{B2})$ (15)

$C_{\theta 2} = C_2 \sin(\alpha_2)$ (16)

$C_{m2} = C_2 \cos(\alpha_2)$ (17)

3.3. Sample of the Calculated Experimental Parameters

The following are sample of the experimentally determined and calculated data at (90% of the maximum speed of rotation), covering all the throttling range from maximum mass flow rate until minimum where the surge symptoms starts to appear. The ambient conditions were: p_{o1} = 76.8 cm hg , T_{o1} = 30.5 C^o

Table (1) Sample of the calculated experimental parameters at speed ratio of 90%

mass corrected	T_{o2} mod	P_{o2} mod	π measured	π_{cal} CFX	π_{cal} Emp	Block	Slip	η_{real}	η_{CFX}	η_{Emp}
1.197	110.4	2.22	2.242	2.284	2.22	0.668	0.856	0.864	0.9	0.865
1.161	111.4	2.23	2.255	2.287	2.22	0.621	0.883	0.854	0.899	0.86
1.052	114.2	2.27	2.289	2.3	2.22	0.699	0.851	0.859	0.9	0.866

4. THEORETICAL PREDICTIONS OF IMPELLER LOSSES

In the present work, theoretical predictions of impeller losses have been done using two computational techniques in order to have wide span comparison with the experimentally obtained results. The first technique uses empirical relations, where the second technique uses 3-D viscous flow solution.

4.1. Empirical Relations

The following paragraphs contains the formulas suggested by the proposed loss model , noting that using the proposed formulas requires solving the flow field at first to determine the flow parameters, which in turn requires pre-knowledge of the system efficiency, whereas system efficiency is our objective to be determined. Therefore, an initial value for the efficiency should be suggested, and then the process is repeated iteratively to determine the right efficiency value.

4.1.1. Incidence losses

Galvas et al. [10] Developed a technique to calculate the optimum incidence angle for compressor impeller. He defined the optimum operating conditions as those, which gives zero blade loading at the leading edge, i.e. which produce no change of whirl (C_θ*r). Figure (3) shows the velocity triangles of the incidence process, from which equations (18) and (19) are

$$\tan\left(\beta_{1\,opt}\right) = U_1 / C_{m1} \qquad (18)$$

$$\tan\left(\beta_x\right) = U_1 / C_{mx} \qquad (19)$$

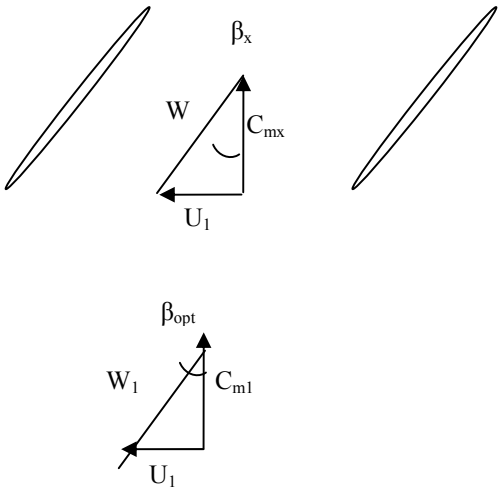

Fig (3), Velocity triangles before and after impeller LE

deduced, then using continuity equation assuming no change in density leads to equation (20).

Galvas also determines the relative velocity component equation (22), where the factor (k) is introduced by Conrad [11] and it ranges from 0.5 to 0.7. Therefore, the non-dimensional stagnation enthalpy losses Δq_i can be calculated using equation (23).

$$\tan\ \beta_{opt} = \frac{AR_1}{AR_x} \tan\ \beta_B \quad (20)$$

$$\left(W_L\right) = W_1\ \sin\left(\left|\beta_1 - \beta_{xopt}\right|\right) \quad (21)$$

$$\Delta h_i = K\ W_L^{\,2}\ /2 \qquad (22)$$

$$\Delta q_i = \Delta h_i / u_2^2 \qquad (23)$$

4.1.2. Skin friction losses

Jansen et al. [12] give the skin friction as equation (24):

$$\Delta q_{sf} = 4\ c_f\ L_h\ \overline{w}^2_y\ d_h\ u_y^2 \qquad (24)$$

Where $\overline{w}$ is the average relative velocity ,L_h is the hydraulic length, dh is the hydraulic diameter defined as four cross sectional area divided by the section circumference, and C_f is the friction factor (can be found from Moody chart) which is applicable to fully developed turbulent flow in straight pipes. Musgrave [13] modifies the friction factor in order to allow for

$$\sigma = e^{-\frac{\Delta s}{R}} = \left[1 - \frac{\gamma - 1}{\gamma R T_{02}} U_2^2 \left(\sum \Delta q\right)\right] \qquad (34)$$

$$cf' = cf \left[\mathrm{Re}\left(d/2R_c\right)^2\right]^{0.05} \qquad (25)$$

curvature effects using equation (25). Where Re = is the mean

$$D = 1 - \frac{W_2}{W_{1rms}} + \frac{\pi r_2\ \Delta q_{th}\ U_2}{Z\ L\ W_{1rms}} + 0.1\ \frac{b}{r_{ss}}\left(1 + \frac{W_2}{W_{1rms}}\right) \qquad (26)$$

flow Reynolds number, Rc = is the mean flow radius of curvature

4.1.3. Diffusion and blade loading losses

It is the loss of momentum due to boundary layer growth. Rodgers [14] proposed the following formula (equation 26) for

$$\Delta q_{th} = \left(C_{\theta 2} U_2 - C_{\theta 1} U_1\right) U_2^2 \qquad (27)$$

Where, L is the blade length along the mean streamline
$b = (r_{1s} - r_{1h} + b_2)/2$ and $r_{ss} = r_2 - r_{1s}$

the diffusion factor is given by equation (27), it based on the analysis of experimental data from centrifugal compressors.
Finally, the non-dimensional stagnation enthalpy loss can be calculated using the following relation (equation 28)

$$\Delta q_{bl} = 0.05\ D2 \qquad (28)$$

4.1.4. Clearance Losses

Jansen and Qvale [12] developed the following relationship (equation 29) for the non-dimensional stagnation enthalpy loss due to clearance as:

$$\Delta q_{cl} = 0.6\ \frac{\varepsilon}{b_2}\ \frac{C_{\theta 2}}{u_2}\left\{\frac{4\pi}{b_2 Z}\left(\frac{r_{1s}^2 - r_{1h}^2}{(r_2 - r_{1s})(1 + \rho_2/\rho_1)}\right)\frac{c_{\theta 2}}{u_2}\ \frac{C_{m1}}{u_2}\right\}^{1/2} \qquad (29)$$

He assumed the flow through the clearance gap to undergo a sudden contraction followed by a sudden expansion. Musgrave [13] pointed that the running clearance varies with the operating speed and he suggested the following formula (equation 30).

$$\frac{\varepsilon_c}{b_2} = \frac{\varepsilon}{b_2} - \left(\frac{\alpha}{b_2}\right)\left(\frac{n}{n_{des}}\right)^{2..3} \qquad (30)$$

Where ε is the stationary clearance
ε_C is the operating clearance
α Constant $(0.016 - 0.027)*10^{-3}$

4.1.5. External losses

In addition to the internal flow losses described above, there exists another kind of losses called external losses, which is defined as the rise of the impeller discharge stagnation enthalpy without any corresponding increase in pressure. They are usually classified as disc-friction and recirculation losses, but they can also include any heat transfer from external sources. Daily and Nece [16] quoted an approach to determine the non-dimensional stagnation enthalpy loss, the approach based on experimental investigation of the power required to rotate discs in an enclosed space, they used the following formula (equation 31):

$$\Delta q_{df} = 2.5\ \rho U_2\ r_2^2\ kf\ /\ \dot{m} \qquad (31)$$

Where: $kf = 3.7\ (\varepsilon / r_2)^{0.1} / \mathrm{Re}^{.5}$ for $\mathrm{Re} < 3*10^5$
$kf = 0.102\ (\varepsilon / r_2)^{0.1} / \mathrm{Re}^{.2}$ for $\mathrm{Re} > 3*10^5$
Re is the impeller Reynolds number = $U_2\ r_2\ /\nu$

$$\Delta q_{re} = 0.02\ D^2 \sqrt{\tan \alpha_2} \qquad (32)$$

For the recirculation Losses, Jansen and Qvale [12] gives the expression of the non-dimensional enthalpy loss coefficient, as follows:

where D is the diffusion parameter given by equation (26).

Finally, the entropy gain factor (σ) can be calculated using equations (33, and 34), and the efficiency is calculated using equation (35) as stated by Whitfield and Baines [7].
The loss model was examined through determination of the efficiency and pressure ratio of a real compressor then

$$\sum \Delta q = \Delta q_{i} + \Delta q_{sf} + \Delta q_{bl} + \Delta q_{cl} + \Delta q_{df} + \Delta q_{re} \qquad (33)$$

comparing between the loss model results and experimental data, which shows a good agreement as shown in table (1).

4.2. 3-D Viscous Flow Solution

$$\eta_{tt} = \frac{\sigma^{\frac{\gamma-1}{\gamma}}\left(1-\left(\frac{P_{o1}}{P_{o2}}\right)^{\frac{\gamma-1}{\gamma}}\right)}{1-\left(\frac{\sigma P_{o1}}{P_{o2}}\right)^{\frac{\gamma-1}{\gamma}}} \qquad (35)$$

CFX-BladeGen software is one of the most famous packages for solving the fluid flow field in turbo machinery applications. The used version in the present work is V 4.1. This software solves the fluid flow governing equations using the finite volume method; the used turbulence model in this version is the zero equation. Many authors have used this software and they reported good agreements between its solution and their experimental work. Banini E. [13] compared between the flow field solution using CFX-BladeGen software and a published measurements for the same cases. Khalil et al. [14] used this software for solving the flow field around an axial fan. Mizuki et al. [2] published detailed measurements of a three centrifugal compressors using yaw probes for measuring total and static pressure along the channel between blades. Elnashar et al. [15] compared between that measured data and the corresponding calculations using CFX-BladeGen software, and they reported a good agreement.
Figure (4) shows sample of the grid generated by CFX-BladeGen for the engine 4M-1 impeller. The samples include steam wise, meridional, and span wise cuts respectively.
Figure (5) shows the engine 4M-1 impeller and its measuring device for determination of r, θ, and z coordinates. Figure (6) shows contours of relative Mach number for hub to shroud and blade-to-blade planes for the same impeller, determined by CFX-BladeGen. Figure (7) shows contours of relative total pressure for hub to shroud and blade-to-blade planes for the same impeller, determined by CFX-BladeGen.

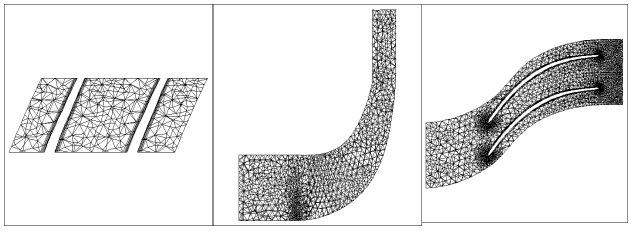

a **b** **c**

Fig (4) Samples of the grid generated by CFX-BladeGen program, a-stream wise,
b- Meridional and c- span wise cuts respectively

Fig (5), the engine 4M-1 impeller and its measuring device for obtaining of r, θ, z coordinates.

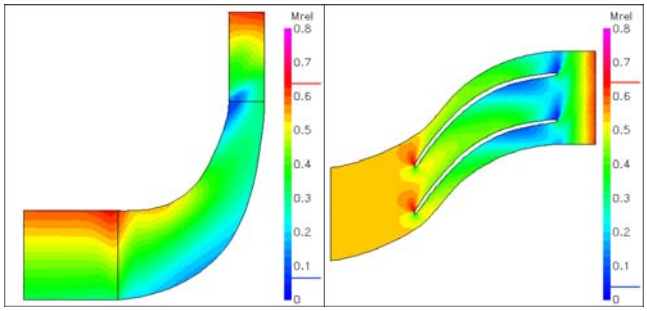

Fig (6) Contours of relative Mach number
for hub-to-shroud and Blade-to-blade planes,
obtained by CFX-BladeGen.

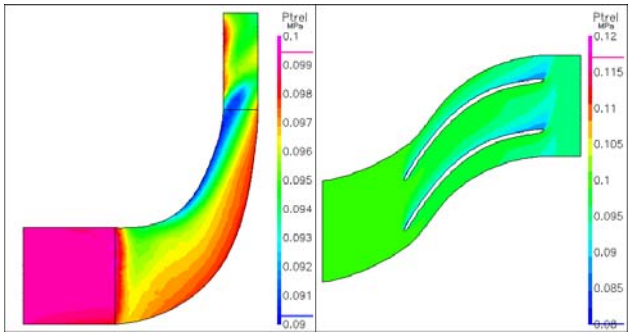

Fig (7) Contours of relative total pressure for hub-to- shroud and Blade-to-blade planes, obtained by CFX-BladeGen.

5. RESULTS AND DISCUSIONS

A comparison between the results, which are obtained by measurements and those obtained by the proposed methods are shown in figure (8), the upper part indicate the total-to-total efficiencies and the lower part indicate the pressure ratios at corresponding mass flow rate and speed ratios. The speed ratio is varying from 50% to 90% by a step of 10 %.

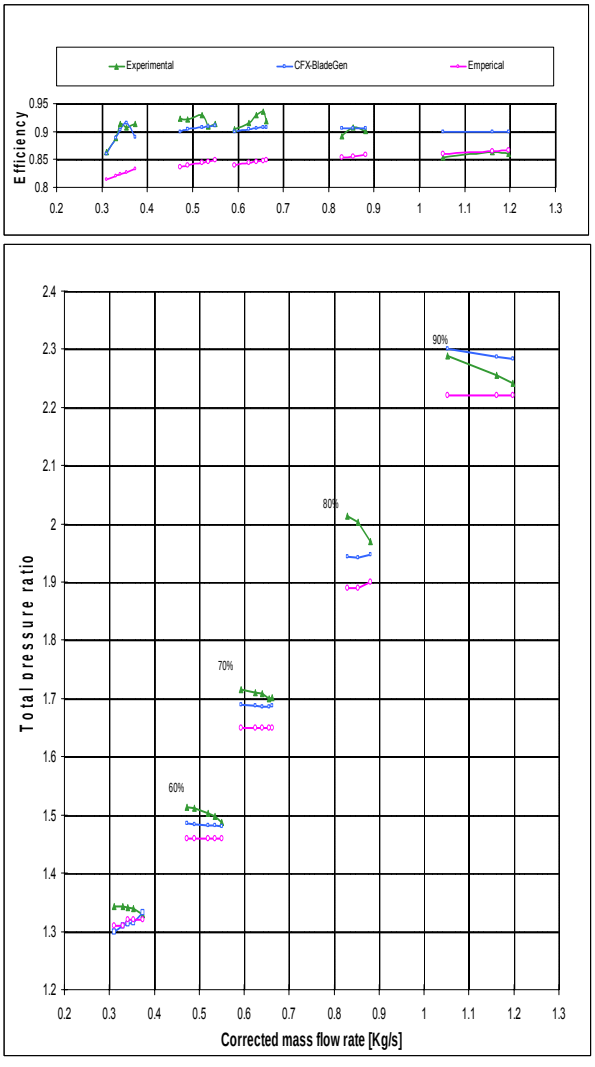

Fig (8) Impeller characteristics map

The deviation errors in the pressure ratio between the theoretical and experimental results are shown in figure (9). The maximum and minimum deviation values are occurring at almost the same mass flow rate. The maximum deviation error of empirical and CFX-BladeGen solutions are found to be -6.29 and -3.28 % respectively at speed ratio of 80% and corrected mass flow rate from 0.85 to 0.825 kg/s. The minimum deviation error is found to be 0.0 and + 0.3 % respectively, at low speed ratio of 50% and at the same mass flow rate of 0.38 kg/s. At speed ratio of 90% the deviation error is found to be -1 and + 1.187 % for empirical and CFX-BladeGen solutions respectively.

The error fittings are shown in the same figure, they vary periodically over the corrected mass flow rate band for both empirical, and CFX-BladeGen modeling solutions and they are consistent in phase, i.e. the variation pattern for both solutions occur at almost the same flow rate. The empirical solution error distribution is found to be varying equally around the horizontal error line of -3% with amplitude of ± 2%, while for CFX-BladeGen solution it varies around the zero error line with amplitude of ± 2.2 % at speed ratio range from 60 to 90 %.

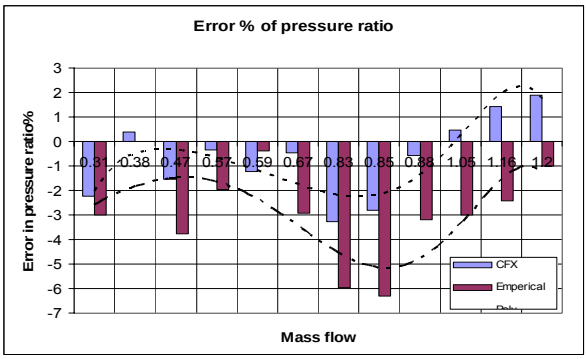

Fig (9) Pressure ratio error distribution of the theoretically obtained Loss models by empirical And 3-D CFX-BladeGen solutions

Fig (10) Efficiency error distribution of the theoretically obtained Loss models by empirical and 3-D CFX-BladeGen solutions

The efficiency error variations are shown in figure (10); they resemble the variations of the pressure ratio. The deviation for empirical solution error is found to be from + 0.7 to - 9.7 % at speed ratios of 90 and 50 % respectively, while for CFX-BladeGen solution is found to be varied from + 5.39 to – 3.26 % at the same speed ratios as empirical modeling. The two error variation patterns are symmetrical around two parallel inclined lines.

6. CONCLUSION

The proposed empirical model and the 3-D viscous flow solver (CFX-BladeGen) are considered very powerful tools for evaluating the losses in the centrifugal compressors, especially the impellers.
The deviation errors of the pressure ratios are found to be vary from (0.0% to - 6.3%) for empirical modeling and from (+ 1.87 to - 3.3 %) for CFX-BladeGen solution respectively at the same corresponding speed ratios.
The deviation errors in the total-to-total efficiency are found to vary from (0.0% to -9.7%) for empirical modeling and from (+ 5.4% to - 3.3 %) for CFX-BladeGen solution at the same corresponding speed ratios with variation pattern resemble to that obtained for pressure ratio.
The theoretical results show good agreement with the used impeller, but for CFX-BladeGen, the result is excellent, so it can be used for simulation in the cases having nearly the same mass flow rate, pressure ratio and dimensions for saving efforts and test rig construction and running costs.
Measuring total pressure, static pressure, and total temperature at the compressor outlet can be used to calculate the compressor efficiency with high accuracy. Whereas calculating the slip factor and aerodynamic blockage using this measured data can give good results near the design conditions, it is not recommended to be used at the off design conditions. The reason is the partial flow stagnation due to high incidence at diffuser, and the long calculation procedure with possible associated error accumulation through them.

7. NOMENCLATURE

a = sonic speed
AR = area
b = blade height
BL = blockage (useful percentage of the geometric area)
C = absolute velocity
Cf = friction factor
D = diameter, diffusion factor
Emp = empirical
M = mach number
m = mass flow rate
mf = mass flow parameter (mf = Vmean / Vmax)
n = rpm
P = pressure
R = gas constant
Re = is the mean flow Reynolds number
Rc = is the mean flow radius of curvature
r = radius
rms = root mean square value
T = temperature
th1 = blade thickness at inlet
th2 = blade thickness at outlet
U = peripheral speed
W = work
w = relative velocity
x = just after impeller inlet
y = just after impeller exit
z = number of blades

Latin
α = absolute flow angle
β = relative flow angle
γ = angle / specific heat ratio
ρ = density
μ = slip factor
η_i = impeller efficiency

Subscripts
0 = upstream conditions
1 = compressor inlet
2 = compressor outlet
22 = down steam the impeller outlet by 6 mm
3 = combustion chamber
4 = exhaust duct
B = blade
cal = calculated
h = hub, hydraulic
in = intake
inf = for infinite number of blades
m = meridional
o = total conditions
r = relative
s = static, shroud
θ = peripheral direction

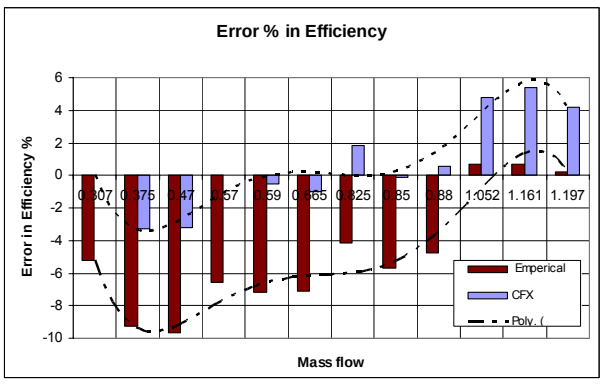

8. RFERENCES

[1] Ecardt D.,"Flow Field Analysis of Radial and Back swept Centrifugal Compressor Impellers", Part 1, "Flow Measurements Using a Laser Velocimeter". symposium on performance Prediction of Centrifugal Pumps & Compressors, In Proceedings of the ASME 25th Annual International Gas Turbine Conference and 22nd Annual

Fluids Engineering Conference on *Performance Prediction of Centrifugal Pumps and Compressors*, New Orleans, Louisiana, March 1980, pp. 77–86

[2] Mizuki S., Ariga I., Watanabe I., “A Study of Flow Mechanism within Centrifugal Impeller Channel”. ASME T4-GT-14, December 1975.

[3] Elnashar, A. Abdelrahman M. Hashim, A. Eldalil, K. "Theoretical and Experimental Study of Centrifugal Compressors", thesis master of science in Aerospace engineering, Cairo university, Cairo 2001.

[4] Eldalil, K, Ph.D. thesis, "Theoretical and Experimental Investigation of Radial Turbomachines", MTC Cairo 1991.

[5] Wisner, F. J., "Review of Slip Factor for Centrifugal Impellers Trans ASME Journal of Engineering for Power ", 89 558, 1967.

[6] Pampreen R.C, "A Blockage Model for Centrifugal Compressor Impellers ", Transactions of the ASME 698/vol 103, October 1981.

[7] Whitfield A, Baines N.C, "Design of Radial Turbo machines" Longman Group UK Limited, 1990.

[8] Cumpsty N.A, "Compressor Aerodynamics", 1989

[9] Mattingly D., "Elements of Gas Turbine Propulsion", 1996.

[10] Galvas, M. R. "Fortran Program For Predicting Off-Design Performance Of Centrifugal Compressors ". NASA TN D-2621, 1973.

[11] Conrad, O., Raif, k., and Wessels, M., "The Calculation of Performance Maps for Centrifugal Compressors with Vane-Island Diffusers" ASME 22nd fluids engineering conference.1980

[12] Jansen W, Qvale, E. B. 1967 “A Rapid Method for Predicting the off Design Performance of Radial Inflow Turbines" ASME paper 67-WA/GT-3, Cambridge, 1967

[13] Benini E. “Optimal Navier Stokes Design of Compressor Impellers Using Evolutionary Computation”. International Journal of Computational Fluid Dynamics, October 2003 Vol. 17(5), pp. 357.369

[14] Khalil, M. K. Alzahaby A, “Automation of wind Tunnel Operation”, Thesis of Master of Science MTC, Cairo 2003.

[15] Elnashar A., Abdelrahman M.,”Design Optimization of Centrifugal Compressor Impellers”. PhD thesis Cairo University, January 2008

[16] Daily J W, Nece R E “chamber dimension effects on induced flow and frictional resistance of enclosed rotating disk", Trans ASME journal of basic engineering (82:217) 1960.